Metal-Organic Framework/Graphene Oxide composites for CO_2 capture by Microwave Swing Adsorption

Mégane Muschi[a], Sabine Devautour-Vinot[b], Damien Aureau[c], Nicolas Heymans[d], Saad Sene[a], Rudolf Emmerich[e], Alexandros Ploumistos[a], Amine Geneste[b], Nathalie Steunou[a,c], Gilles Patriarche[f], Guy De Weireld[d], Christian Serre*[a]

a. Institut des Matériaux Poreux de Paris, ESPCI Paris, Ecole Normale Supérieure, CNRS, PSL University, 75005 Paris, France.
Email : christian.serre@espci.psl.eu
b. ICGM, Univ. Montpellier, CNRS, ENSCM, Montpellier, France.
c. Institut Lavoisier de Versailles, UMR 8180 CNRS, Université de Versailles St Quentin en Yvelines, Université Paris Saclay, Versailles, France.
d. Service de Thermodynamique et de Physique mathématique, Faculté Polytechnique, Université de Mons, 7000 Mons, Belgium.
e. Fraunhofer Institute for Chemical Technology ICT Joseph-von-Fraunhofer St. 7, 76327 Pfinztal, Germany.
f. Université Paris-Saclay, CNRS, Centre de Nanosciences et de Nanotechnologies, 91120, Palaiseau, France.

Abstract

Metal-organic frameworks (MOFs)/Graphene oxide (GO) composites are of growing interest due to their properties which can exceed those of the pure components, including post-combustion CO_2 capture. Series of composites suitable for CO_2 capture under flue gas conditions based on the microporous water stable MIL-91(Ti) have been prepared with different GO contents, following two routes, *in situ* and post-synthetic. It was observed that the 5wt% GO *in situ* composite exhibits a semi-conducting behavior, while the post-synthetic materials are insulating, even with high

(20wt%) GO content. As a consequence, this composite absorbs microwave radiation more efficiently compared to the pure MOF and post-synthetic materials. Finally, we report that CO_2 desorption is much faster under microwave irradiation compared to direct electric heating on MOF/GO *in situ* materials, paving the way for future energy-saving Microwave Swing Adsorption processes.

Introduction

Metal-organic frameworks (MOFs)/Graphene oxide (GO) composites have recently attracted a lot of attention due to the synergic effects between the two materials, leading to enhanced properties compared to the individual components.[1-3] It has for instance been shown that MOF/GO composites can exhibit higher porosity than the parent MOF and are suitable candidates for gas adsorption, including CO_2 capture.[4-7] In post-combustion industrial processes, the use of adsorbents usually involves pressure swing adsorption (PSA) or thermal swing adsorption (TSA) processes. The latter consists of using steam or hot gas sent into the separation column during the desorption step to regenerate the material through thermal transfer between the steam/hot gas and the adsorbent. This process allows for a lower energy penalty compared to other regeneration methods when dealing with relatively low CO_2 content as in post-combustion processes.[8, 9] However, it requires a uniform and fast heating rate of the material in the separation column. Unfortunately, MOFs exhibit very low thermal conductivities and the use of TSA (direct heating with steam or gas) or conventional electric heating (direct electric heating of the column through Joule effect, namely the Electric Swing Adsorption process[10]) is associated with slow desorption kinetics, which limits the practical use of MOFs despite their suitable adsorption properties. Therefore, there is a need to find more efficient alternative desorption processes that would decrease the energy penalty related to the material regeneration. Among reported innovative desorption processes, the use of microwave irradiation, called microwave swing adsorption (MSA), has proven to lead to faster CO_2 release compared to conventional heating on solid adsorbents such as activated carbons.[11] Also, Lee *et al.* have shown that the use of microwave radiation can be more efficient compared to conventional heating for MOF activation.[12] Therefore, these electromagnetic radiation should lead to faster CO_2 release compared to thermal or electrical heating, without damaging the adsorbent.

However, except for a few conductive 2D-MOFs that are not really suitable for CO_2 capture due to their lack of interactions with CO_2, their high cost and their poor hydrolytic stability,[13,14] MOFs usually exhibit very low electrical conductivity, associated with low dielectric losses and low microwave heating[15] that would hamper their use for MSA processes.

By combining them with graphene oxide or reduced graphene oxide, the electrical conductivity can however be significantly enhanced, which is of interest for CO_2 capture through the MSA process but also for the development of new batteries, supercapacitors or to address catalytic challenges[2] .

To date, several synthetic methods to prepare MOF/GO materials have been reported.[3] The most common routes are the *in situ* and the post-synthetic (*ex situ)* methods. The first one consists of mixing the MOF's precursors with GO prior to using the conditions required for the MOF synthesis. In this case, some of the oxygen-bearing groups of GO form coordination bonds with the metal of the MOF and hence act as nucleation sites for the MOF growth.[16-18] The second method consists of mixing the pre-formed MOF particles with GO nanosheets, usually at a pH value at which the two materials exhibit oppositely charged surfaces to allow for electrostatic interactions. To our knowledge, only one study has compared these two types of composites in terms of microstructure and catalytic properties and has shown that they both strongly depend on the preparation route.[19] However, the electrical conductivity of these composites has never been compared. Recently, some of us have shown that the *in situ* formation of MIL-69(Al) in the presence of GO can lead to core-shell MIL-69(Al)-GO nanostructures. The peculiar microstructure of this composite strongly impacts their electron transport properties.[20]

Here, in order to develop suitable MOF/GO composites for CO_2 capture using the MSA process, displaying both a good CO_2 adsorption capacity and semi-conducting behavior, we report the synthesis via *in situ* and post-synthetic routes of new MOF/GO composites with different GO contents. The water stable microporous Ti bisphosphonate MIL-91(Ti) that has already been shown to be promising for post-combustion CO_2 capture was selected.[21] We report first that *in situ* and post-synthetic materials exhibit significant differences in terms of electrical conductivity and microwave absorption properties, in relation to the composites' respective microstructures. Finally, as a proof of concept, we evidence the faster CO_2 desorption rate under microwave radiation compared to conventional heating on microwave absorbing MIL-91(Ti)/GO *in situ* composite. Such result was also observed for another *in situ* composite based on a MOF exhibiting a different structure and chemical composition from MIL-91(Ti), namely UiO-66-btc(Zr). We therefore believe that these *in situ* composites are of strong interest for the future design of MSA based CO_2 capture processes (Figure 1).

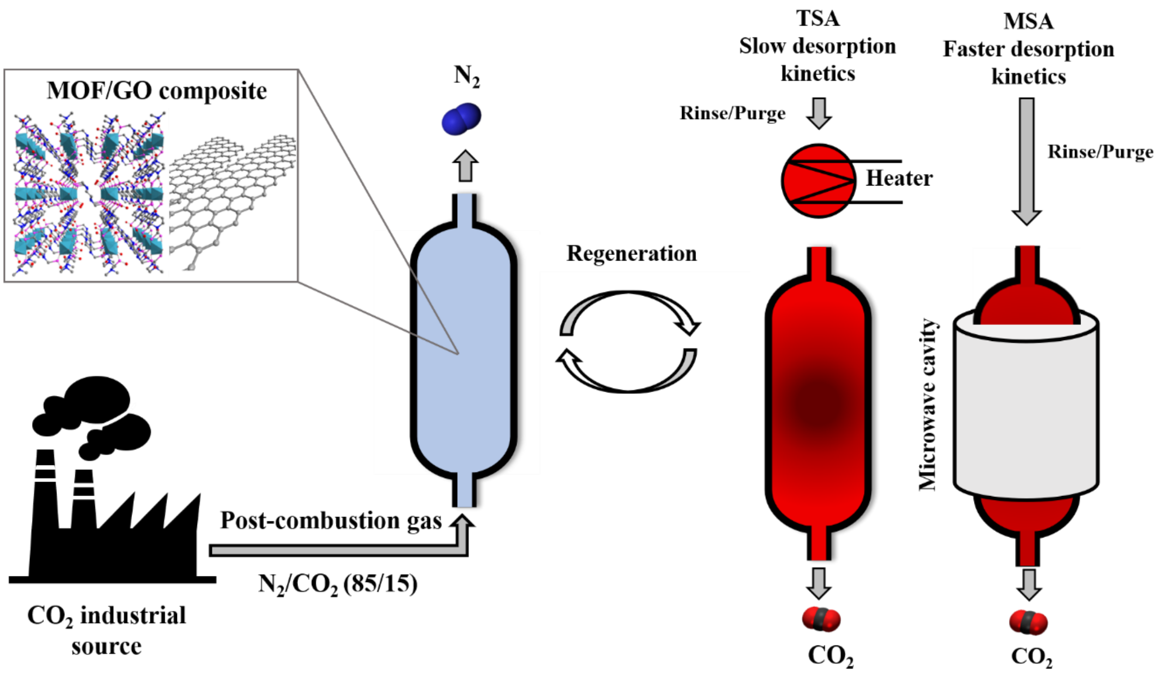

Figure 1. Schematic illustration of the MSA process compared to the TSA process on MOF/GO composites, illustrated with MIL-91(Ti)/GO, for CO_2 post-combustion capture.

Experimental

Materials

Graphene oxide was purchased from Graphenea S. A. $TiO(acac)_2$, $ZrCl_4$, benzene-1,2,4-tricarboxylic acid, piperazine 99 %, hydrochloric acid 18%, formaldehyde and acetic acid 99 % were purchased from Alfa Aesar. Phosporous acid was purchased from Acros.

Syntheses

N,N'-piperazinebismethylenephosphonic acid. Piperazine (103 g, 1.2 moles), phosphorous acid (196 g, 2.4 moles), water (600 mL) and a solution of HCl 18 % (600 mL) were introduced in a 5 L reactor. Formaldehyde (389 g) was added dropwise and the reaction was put under stirring at 120

°C for 3 h 30. The white solid was collected by filtration and dried at 100 °C under vacuum (180 g, 0.7 moles, 58 %).

MIL-91(Ti). N,N’-piperazinebismethylenephosphonic acid (1.14 g, 4.2 mmol) was dissolved in 30 mL water. The solution was stirred and put at 70 °C for 15 minutes. $TiO(acac)_2$ (1.09 g, 4.2 mmol) was added and the reaction was put under reflux for 16 h. The white solid was collected by filtration, washed with water and ethanol and dried under vacuum at 100 °C (1.3 g, 3.8 mmol, 90 %).

MIL-91/GO post-synthesis composite. GO (5, or 20wt% compared to the MOF) was dispersed by sonication in 40 mL water. The pure MOF was added (pH = 2.8) and the suspension was stirred for 4 h. The grey solid was collected by filtration, washed with water and dried under vacuum.

MIL-91/GO in situ composite. The linker (1.14 g, 4.2 mmol) was dissolved in 30 mL water and the solution was put under stirring at 70 °C for 15 minutes. $TiO(acac)_2$ (1.09 g, 4.2 mmol) was then added and the reaction was put under reflux. After 6 h, the GO (2, 5, 10 or 20wt%) was dispersed in 30 mL water by sonication and added to the reaction which was let under reflux for an additional 16 h. The grey solid was collected by filtration, washed with water and ethanol and dried under vacuum.

UiO-66-btc(Zr). $ZrCl_4$ (2.4 g, 10.3 mmol), benzene-1,2,4-tricarboxylic acid (4.2 g, 20 mmol), water (60 mL) and acetic acid (6 mL) were introduced in a 100 mL round bottom flask. The solution was put under reflux for 24 h. The white solid was collected by filtration and dried at 50 °C to avoid the formation of anhydride.

UiO-66-btc(Zr)/GO post-synthesis composite was synthesized using the same procedure as for MIL-91/GO post-synthesis composites except that the pH was set at 1.6 using a HCl solution.

UiO-66-btc(Zr)/GO in situ composites were obtained by using the same procedure than for pure UiO-66-btc(Zr) with the addition of 5, 10 or 20wt% GO to the MOF precursors prior to starting the reflux.

Shaping

3wt% polyvinyl butyral was dissolved in ethanol and added to the MOF powder. The mixture was mixed vigorously and shaped by rolling the powder in a spherical vessel. The beads were then dried at 80 °C and sieved. Only the beads of diameter between 1 and 2 mm were kept.

Results and Discussion

Characterizations

MIL-91(Ti) is a microporous Ti(IV) bisphosphonate MOF made of corner-sharing chains of titanium octahedra connected by a piperazine bis-phosphonate linker delimiting narrow 1D pore (ϕ ≈ 4Å) channels (Figure 2).[22] This solid, together with its Al analogue MIL-91(Al), is a rare example of a 3D metal phosphonate MOF that has shown promising results for post-combustion CO_2 capture with a high CO_2/N_2 selectivity and CO_2 adsorption capacity.[21] This hydrothermally stable material was also synthesized using green conditions according to a modified literature procedure (see Experimental section).[21]

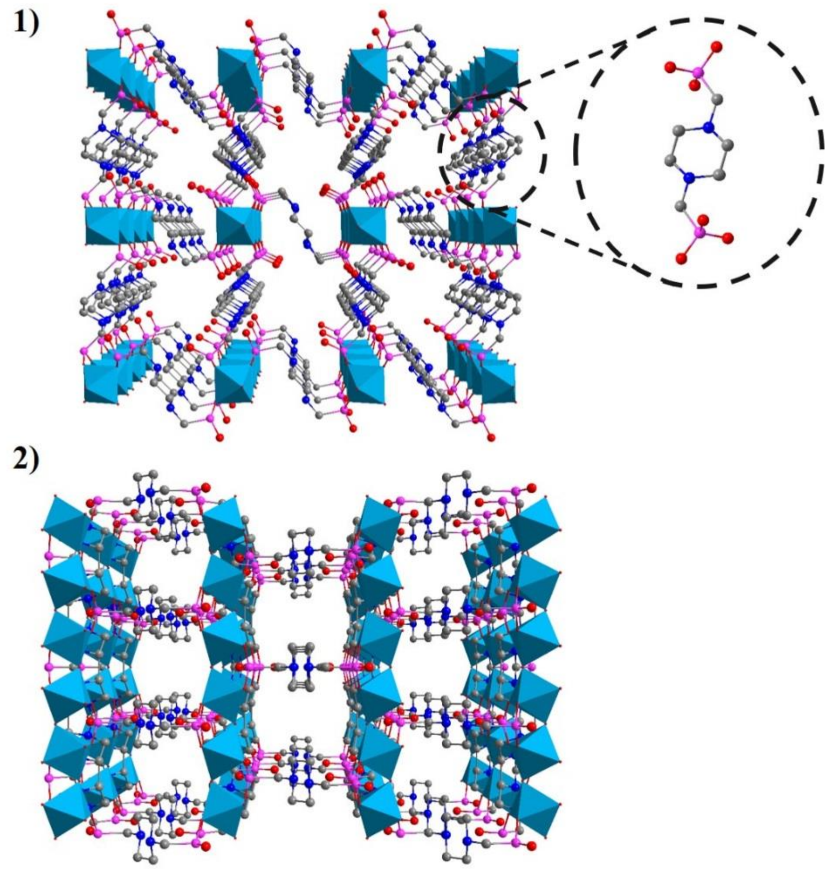

Figure 2. Crystal structure of MIL-91(Ti) along the 1) b axis with the structure of the linker 2) c axis. The titanium octahedra are represented in blue, the carbon, oxygen, nitrogen, phosphorus atoms in grey, red, dark blue and pink, respectively.

To optimize the sorption and physical properties of the composites for their use in CO_2 capture using MSA, *in situ* and post-synthesis MOF/GO materials were synthesized using variable amounts of GO (2-20 wt %). They will be denoted as MOF/GO*x*wt% where *x* is the theoretical mass of GO compared to that of the MOF.

To obtain the MIL-91(Ti)/GO post-synthesis composites, the zeta-potential of the pure components was first measured in deionized water to determine a pH range for which the two materials' surfaces (MOF, GO) are oppositely charged (Figure S4). Then, the MOF was dispersed in water and mixed with a specific amount of GO at room temperature under a controlled pH value, close to 2.5, to promote the self-assembly of the two materials through electrostatic interactions.

The preparation of MIL-91(Ti)/GO *in situ* composites was also investigated. Similar synthetic conditions as of the pure MOF were first considered, as reported for other MOF/GO *in situ* composites.[4, 5, 18, 23-29] The MOF's precursors were thus mixed with the GO nanosheets in water at room temperature prior to heating the mixture overnight under reflux. However, these conditions led to MOF/GO composites with a large amount of unreacted linkers, suggesting a competition between the oxygen-bearing groups of GO and the MOF linker to react with the metal species. Therefore, alternative synthetic conditions were investigated, specifically adding the GO nanosheets dispersed in water to the reaction medium after the initial stage of the MOF's nucleation had begun, here after 6 hours under reflux. The reaction mixture was then left for an additional 16 hours under reflux.

The resulting composites were characterized by PXRD. As shown in Figure S5 the composites' patterns are similar to that of pure MIL-91(Ti), giving evidence of the successful *in situ* crystallization of the MOF. Note that the Bragg peak related to the [001] plane of pure GO, at 10.3°, is not observed for any of the composites. This suggests that for both types of composites, the long-range stacking of GO sheets is lost, in agreement with a disordered intercalation of some MOF's particles between the nanosheets. Also, for the *in situ* composites, the Bragg peaks width is slightly larger when increasing the GO content (Table S2). Although the particle size distribution is not narrow, this is in agreement with a decrease in particle size evidenced by TEM images (Figure S6). This decrease in size for the *in situ* materials with increasing GO content has been attributed previously to the nucleation of the MOF on some oxygen-bearing groups of GO, limiting the growth of MOF particles related to the Ostwald ripening.[18, 30] It suggests that the *in situ* synthesis successfully led to the formation of coordination bonds between the metal of MIL-91(Ti) and some oxygen-bearing groups of GO. This is in agreement with the higher thermal stability observed by TGA of the *in situ* composite compared to the post-synthetic one (Figure S7).

When comparing the nitrogen porosimetry of the *in situ* and post-synthetic composites with 5wt% GO with that of the pure MOF, higher BET surface areas were obtained for the composites (Figure 3, Table 1). This is due to the creation of microporosity at the MOF/GO interface. Regarding the *in situ* composite, those micropores result from the coordination bonds between the two materials that maintain a close interface, as already discussed by Petit *et al*.[16] It appears that the electrostatic interfacial interactions between the MOF and GO surfaces of the post-synthetic composite also lead to the formation of additional micropores, as already observed for the UiO-66-NH_2(Zr)/rGO post-synthetic material[31]. Those extra-micropores at the MOF/GO interface for the two composites result in higher micropore areas compared to the pure MOF (Table 1).

The effect of the GO content, between 2wt% and 20wt%, on the *in situ* composites' porosity was also studied by nitrogen porosimetry. As shown in Figure 3, the MIL-91(Ti)/GO2wt% *in situ* sample exhibits the highest BET surface area with 422 $m^2.g^{-1}$. With 5wt% GO, a slightly lower BET surface area of 405 $m^2.g^{-1}$ was obtained, higher than that of the pure MOF (370 $m^2.g^{-1}$). When increasing the GO content up to 10 and 20wt%, lower BET surface areas of 228 $m^2.g^{-1}$ and 210 $m^2.g^{-1}$, respectively, were however obtained. This decrease cannot be explained only by the presence of non-porous GO. Therefore, it suggests a partial pore blocking of the MOF's channels by GO nanosheets, particularly when considering the very narrow pores of MIL-91(Ti). This was confirmed by the decrease of the accessible micropore area when increasing the GO content within the composite (Table S3).

Note that to select the most appropriate composite for the MSA process, a compromise between the porosity and microwave absorption properties must be found. Indeed, as GO is the microwave absorber, its content within the composite must be high enough to efficiently heat the bulk of the material under microwave radiation without using an excessive power. Therefore, despite the slightly higher BET surface area of the MIL-91/GO2wt% *in situ* composite, we selected the MIL-91/GO5wt% *in situ* and MIL-91/GO5wt% post-synthetic materials for the next steps of this study.

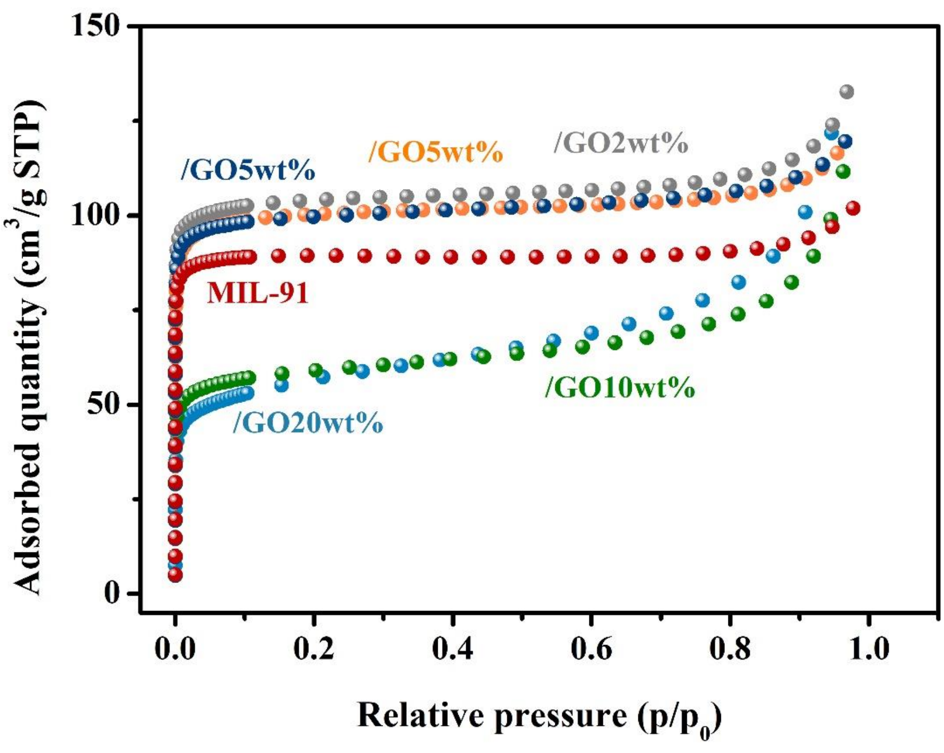

Figure 3. Nitrogen adsorption isotherms at 77 K of MIL-91(Ti) (red), MIL-91(Ti)/GO2wt% *in situ* (grey), MIL-91(Ti)/GO5wt% *in situ* (orange), MIL-91(Ti)/GO10wt% *in situ* (green), MIL-91(Ti)/GO20wt% *in situ* (blue), MIL-91(Ti)/GO5wt%post-synthesis (dark blue).

Table 1. N_2 BET surface area, external surface area, micropore area, micropore volume of MIL-91(Ti), MIL-91(Ti)/GO5wt% *in situ* and post-synthesis (T=77 K, P_0=1 atm.).

	S_{BET} (m^2/g)	S_{Ext} (m^2/g)	S_{Micro} (m^2/g)	V_{Micro} (cm^3/g)
MIL-91(Ti)	370	12	358	0.13
MIL-91(Ti)/GO5wt% *in situ*	405	25	380	0.14
MIL-91(Ti)/GO5wt% post-synthesis	405	25	380	0.14

The 5wt% GO composites were further characterized by electron microscopy. It shows that in both cases (i) MOF particles are in close contact with the GO sheets together with a few isolated bare MOF nanoparticles (Figure S8, S9) and (ii) MOF crystals exhibit a rod-like morphology with a high polydispersity in size (Figure S6.1, S10). Energy-dispersive X-ray spectroscopy (EDS) mapping shows a homogeneous distribution of titanium and phosphorus elements within the MOF crystals with similar Ti/P ratio of 0.50 and 0.48 for the *in situ* and post-synthetic samples, respectively (theoretical value : 0.5) (Figure S11).[21] Noticeably, only the EDS mapping of the *in situ* composite reveals that the GO sheets are covered by phosphorus and titanium atoms, in agreement with the Ti2p XPS spectra that shows two chemical environments (Supporting information, Figure S13). This is in line with a complexation of titanium cations on the oxygen-bearing groups of GO and confirms that those groups act as nucleation sites for the MOF growth, as already observed for other MOF/GO systems.[16, 32-34] In addition, when the synthesis of pure MIL-91(Ti) was carried out under similar concentration conditions than the *in situ* composite (30 mL water at t = 0 min and addition of 30 mL water after 6 hours, see experimental section), the resulting solid was amorphous. This further confirms that the oxygen-bearing groups of GO participate actively to the heterogeneous nucleation and growth of the MOF in these conditions.

SAED measurements performed on the *in situ* composite showed that the MOF growth occurs along the [010] direction, corresponding to the Ti-O-Ti corner-sharing chains of metal octahedra, in agreement with the pores of the MOF being parallel to the GO sheets (Figure S14).

As the main objective here is to design MOF/GO composites with sufficient electrical conductivity for CO_2 capture by the MSA process, the study of the Csp^2 content of GO, that tailors the electron pathway, through XPS C1S spectrum is of particular interest. As illustrated by Figure S15, the C1s spectra of MIL-91(Ti)/GO5wt% *in situ* shows a peak at 284.3 eV that is not observed for the post-synthetic material. This binding energy corresponds to Csp^2, which suggests that GO was partially reduced during the synthesis (see Figure S16 and Table S4 for the XPS C1s spectrum of pure GO). It has been previously reported that GO reduction under heating is more efficient in polar solvents such as water or DMF than in air.[35] To confirm this GO reduction, pure GO sheets were placed in water under reflux overnight. As shown in Figure S17, the GO was indeed slightly reduced, as revealed by the increase of the contribution of Csp^2 compared to the initial GO together with a C/O ratio (from XPS) of 2.4 instead of 2.0 for the initial GO. Therefore, the synthetic conditions of the *in situ* composite lead to a slight reduction of GO that might affect the composites' physicochemical properties.

Electrical conductivity and dielectric properties

To use the composites in the MSA process, the microwave absorption of the material must be high enough to trigger a temperature increase through energy dissipation. The interaction of microwaves with an ideal material that consists of non-interacting dipoles with one relaxation time is described by the Debye relaxation.[15] It is usually expressed by the complex permittivity ε^* that decomposes into a real part (ε'), associated with the energy storage ability of the material and an imaginary part

(ε'') which is related to the dielectric losses and the dissipation of the absorbed energy into heat. They are described according to equation (1) and (2), respectively.

$$\varepsilon' = \varepsilon_\infty + \frac{(\varepsilon_s - \varepsilon_\infty)}{1 + \omega^2\tau^2} \quad (1)$$

$$\varepsilon'' = \frac{(\varepsilon_s - \varepsilon_\infty)\omega\tau}{1 + \omega^2\tau^2} + \frac{\sigma}{\omega\varepsilon_0} \quad (2)$$

With ε_∞ the permittivity at high frequency limit, ε_s the static permittivity, ω the angular frequency, τ the relaxation time, ε_0 is the dielectric constant of free space and σ the electrical conductivity at the angular frequency ω.

The microwave absorption of the material, represented by ε'', depends on its polarizability and electrical conductivity. Therefore, materials suitable for the MSA process should absorb microwave (i) enough to minimize the energy penalty of the process, and (ii) not to such an extent that would disrupt microwave propagation throughout the adsorption column. To achieve this, they must exhibit a semi-conducting behavior. The electrical conductivity of the pure components and composites was measured using complex impedance spectroscopy. As shown by the very low conductivity value ($\sigma < 10^{-8}$ S.cm^{-1} at 373 K) combined with the absence of the σ_{dc} plateau (Figure 4), MIL-91(Ti) is insulating, indicating that no electronic nor ionic charges diffuse over long distances. This behavior is maintained for the post-synthesis composite whatever the GO content, while pure GO shows a semi-conducting behavior ($\sigma_{dc} = 10^{-4.8}$ S.cm^{-1}). The dilution of GO inside the insulating MOF particles induces a poor recovery of the Csp^2 clusters at the sheet-to-sheet junctions, preventing the electron hopping and tunneling of GO.[36] Alternatively, MIL-91(Ti)/GO5wt% *in situ* behaves like a semi-conducting material, with a conductivity value ($\sigma_{dc} \approx 10^{-5}$ S.cm^{-1}) converging towards that of pure GO despite the presence of the insulating MOF as a main phase. This may be due to i) the partial reduction of GO during the synthesis and/or ii) specific MOF/GO interactions allowing to retain the electrical conductivity of pure GO. To examine the first assumption, the electrical conductivity of GO previously soaked in water under reflux overnight was measured. The obtained electrical conductivity is slightly higher than that of pure GO, in agreement with a low reduction degree. It is noteworthy that this increase in value is however too small to explain the higher level of the electrical conductivity of the *in situ* composite compared to that of the post-synthesis one.

Thus, the specific electrical behavior of the *in situ* composite most probably arises from its peculiar microstructure. The formation of this composite involves a direct complexation of Ti cations on the oxygen-bearing groups of GO, followed by the crystal growth, most probably on the sp^3 regions of the GO sheets. In addition, the reflux itself leads to the removal of oxygen atoms that are not coordinated to the MOF, leading to the creation of additional sp^2 clusters, free from any insulating MIL-91(Ti) crystals. As a consequence, the MOF particles most likely do not interfere with the electron hopping of GO that occurs between the sp^2 regions, leading to a material with similar electrical conductivity to pure GO.

The imaginary part of the dielectric permittivity of pure MIL-91(Ti), GO and the two composites with 5wt% GO was then measured at the microwave frequency of 2.45 GHz from 20°C to 120°C with the cavity perturbation method (Supporting information). As shown in Figure S18, MIL-91/GO5wt% *in situ* exhibits a higher value of the imaginary part (ε'') compared to that of the post synthesis composite, which is consistent with the electrical conductivity results.

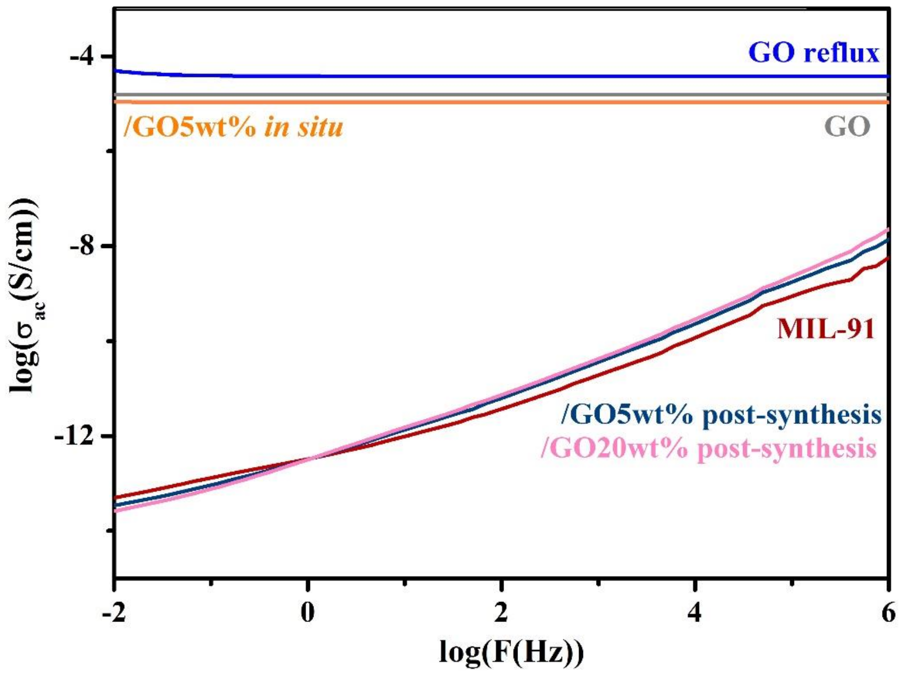

Figure 4. Real part of the conductivity as a function of the frequency recorded at 373 K for GO, GO after 16 h under reflux in water, MIL-91(Ti), MIL-91(Ti)/GO5wt% and 20wt% post-synthesis and MIL-91(Ti)/GO5wt% *in situ*.

Breakthrough curves and CO_2 desorption under conventional and microwave heating

Considering the larger microwave absorption and suitable porosity of the MIL-91(Ti)/GO5wt% *in situ* composite, this material was selected for the CO_2 desorption under microwave irradiation tests. Note that these experiments are a proof of concept of the MSA process based on MOF/GO *in situ* composites. The impact of several parameters (heat transfer, temperature, flow rate) is beyond the scope of this study and will be reported elsewhere.

First, the pure CO_2 isotherm of the composite was measured and compared to that of the pure MOF. The composite exhibits a higher CO_2 adsorption (Figure S19, Table S5), in agreement with its higher micropore area (Figure 3, Table 1). This increase of CO_2 adsorption was already observed for other MOF/GO systems and was attributed to the adsorption of CO_2 molecules not only within the MOF porosity, but also within the micropores at the MOF/GO interface.[5, 37-39]

To avoid any significant pressure drop effects inside the separation column during the desorption tests, the powder was shaped through wet granulation using 3wt% of polyvinyl butyral as the binder, yielding 1 to 2 mm size beads. As shown in Figure S19, the single CO_2 adsorption isotherms revealed an adsorption capacity for MIL-91/GO5wt% spheres a bit lower compared to the powder, in agreement with a slight pore blocking by the polymeric binder (Table S5).

The co-adsorption measurements were performed by saturating the column with a CO_2/N_2 15/85 mixture at a flow rate of 2 NL/h under atmospheric pressure and at 30 °C. When saturation is reached, the material is filled by the gas molecules which leads to the detection of what was injected in the column *e.g* 15 % molar CO_2 and 85 % N_2. The desorption was then carried out under conventional heating (direct electric heating) at a heating ramp of 0.9 °C/sec and under microwave irradiation at approximately 50 °C (Supporting information). The temperature was monitored by an infrared camera for the MW desorption and by a temperature probe for conventional heating (Figure S20). To reach the desorption temperature, a continuous MW power of 250 W was required. As shown in Figure 5.2, CO_2 is completely desorbed after 150 seconds under irradiation, significantly faster than under conventional heating which required 240 seconds. The adsorption/desorption cycles are reproducible under both conventional heating and MW radiation, giving evidence that the desorption processes do not damage the composite and that the adsorption capacity is maintained (Table S6). However, the cyclability under MW radiation shall be investigated over more cycles in the near future to confirm the long-term stability and efficiency. Noticeably, desorption under conventional electrical heating was also performed at 80 °C and led to a desorption time of 215 seconds, longer than what was obtained under MW radiation at ~ 50 °C (Figure S21).

To investigate whether this faster CO_2 desorption under the MSA process is specific or not to MIL-91(Ti)/GO *in situ* systems, composites were synthesized with another MOF exhibiting a different structure and composition (metal, linker), namely UiO-66-btc(Zr).[40, 41] This MOF is a zirconium(IV) oxo-cluster tri-carboxylate material with a cubic architecture delimiting two types of microporous cavities and which possesses free COOH groups suitable to interact specifically with CO_2 molecules (Figure S22).[42] Similarly to the MIL-91/GO composites, the UiO-66-btc(Zr)/GO *in situ* composite exhibits a higher microwave absorption (ε'') compared to the post-synthetic material and pure MOF (Figure S25). The desorption time under microwave radiation at ~ 40 °C is again shorter (approximately 120 sec) compared to the desorption time under conventional electrical heating (approximately 210 sec) at the same temperature (Figure 5.4). Breakthrough desorption curves under conventional heating at 50 °C were also measured and showed that the desorption time is longer compared to that under MW radiation at ~ 40 °C (Figure S27). Therefore, it confirms that the faster CO_2 release under MW irradiation is not governed by the nature of the MOF itself but rather by the specific structure of *in situ* composites. The good cyclability of the measurements was evidenced by the superimposition of the breakthrough curves and similar adsorbed and desorbed CO_2 amounts over the cycles (Table S7).

These results undoubtedly confirm that MW desorption is faster than conventional heating, even at lower desorption temperatures. It can be attributed to a higher heating rate as well as a more uniform heating. Indeed, under conventional heating, the sides of the column are heated first, followed by a slow heat transfer from the sides to the material at the center. On the other hand, MW radiation causes a volumetric heating of the material and is thus more efficient and uniform on these composites. These results evidence that the use of microwave absorbing MOF/GO *in situ* materials is a promising strategy for CO_2 capture by microwave swing adsorption processes.

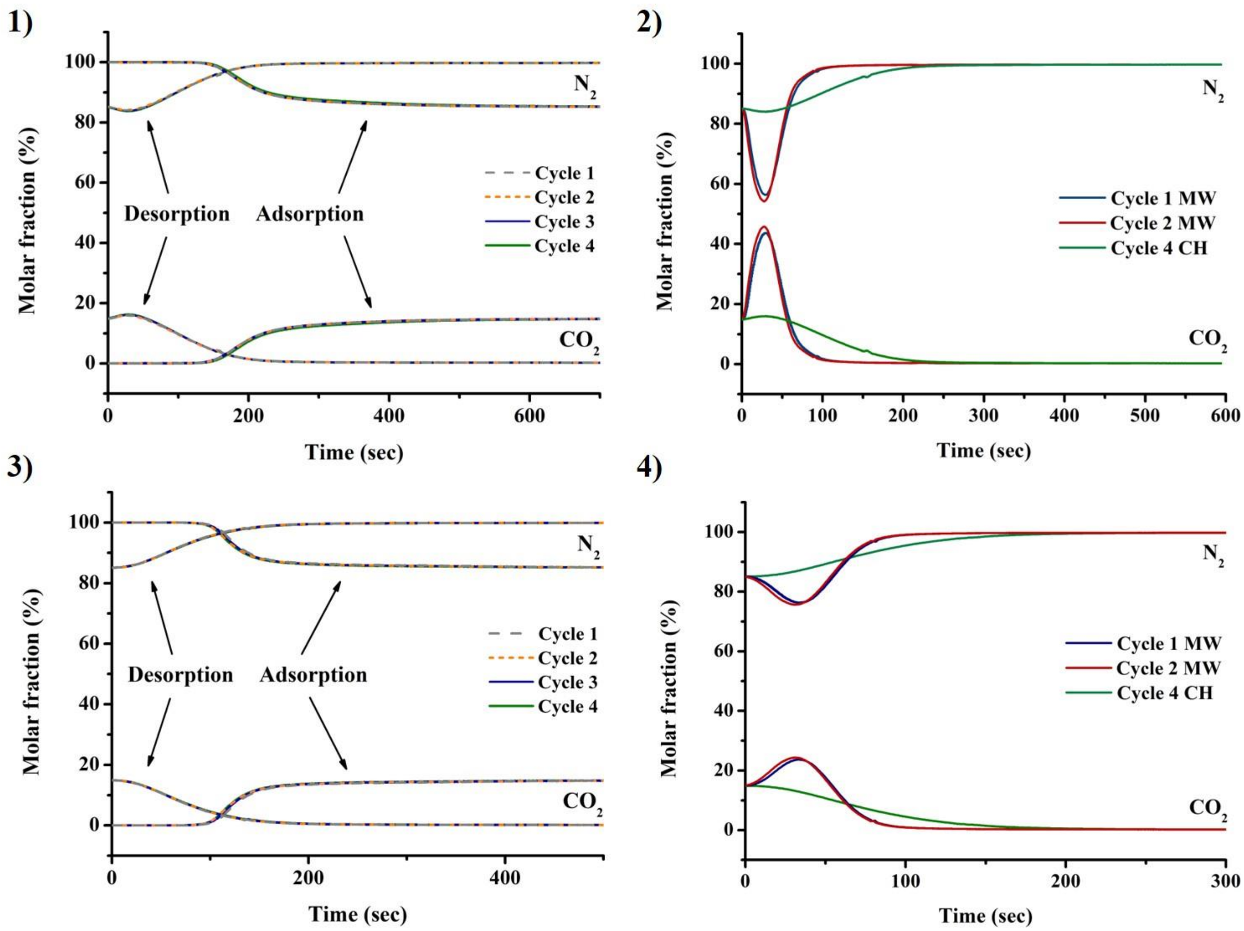

Figure 5. Breakthrough adsorption (mixture CO_2/N_2 15/85 molar, atmospheric pressure, 30 °C) and desorption curves under conventional heating (CH) over 4 cycles at 1) at 50 °C on MIL-91/GO5wt% *in situ* 3) at 40 °C on UiO-66-btc(Zr)/GO10wt% *in situ*. Breakthrough desorption curve obtained under MW radiation and CH 2) at 50 °C on MIL-91/GO5wt% *in situ* 4) at 40 °C on UiO-66-btc(Zr)/GO10wt% *in situ.*

Conclusion

MOF/GO composites suitable for CO_2 capture based on the robust microporous MIL-91(Ti) material have been prepared with different GO contents following different synthetic strategies, *in* *situ* and post-synthetic. We have shown that the *in situ* composite with 5wt% GO exhibits suitable electrical properties for the MSA process. Indeed, the selective growth and crystallization of the MOF over the sp^3 areas of GO induces a specific microstructure for which the insulating MOF particles do not disturb the electron hopping between the sp^2 clusters of GO. Therefore, MIL-91/GO5wt% *in situ* exhibits a semi-conducting behavior whereas post-synthesis composites are insulating, even with relatively high GO content. Finally, the MIL-91/GO5wt% *in situ* composite was evaluated for CO_2 capture with a desorption under microwave irradiation. A much faster release of CO_2 at low temperature (50 °C) under microwave irradiation compared to conventional heating was observed. Similar results were obtained with another MOF/GO *in situ* composite based on the UiO-66-btc(Zr) structure, highlighting the versatility of our strategy. It evidences the great potential of these composite materials for CO_2 capture by MSA process.

Author contributions

M. Muschi synthesized and characterized of pure MIL-91(Ti) and the MIL-91(Ti)/GO composites and participated in the writing of this article. S. Devautour-vinot performed and analyzed the electrical conductivity measurements and contributed to the writing of this article. D. Aureau performed and analyzed the XPS measurements. N. Heymans performed the breakthrough experiments and helped with the writing of this article. S. Sene synthesized and characterized pure UiO-66-btc(Zr) and the UiO-66-btc(Zr)/GO composites. R. Emmerich carried out the desorption under MW radiation experiments in collaboration with N. Heymans and G. De Weireld. A. Ploumistos contributed to the preparation and characterization of the MIL-91(Ti) samples. A. Geneste contributed to the electrical conductivity measurements. N. Steunou helped in the interpretation of the data and the writing of this article. G. Patriarche carried out the HRTEM and

EDS measurements. G. De Weireld supervised the breakthrough adsorption and desorption experiments and helped with the writing of this article. C. Serre was the coordinator of the study and supervised the writing of this article.

Conflicts of interest

The authors declare no competing interests.

Acknowledgements

The authors would like to acknowledge the EU Research and Innovation program Horizon 2020 (H2020/2014-2020) for funding the research presented in this article under Grant Agreement No. 727619 (project Gramofon). The authors would like to acknowledge B. Alonso, A. Ortega from Graphenea S. A. (www.graphenea.com) for providing the graphene oxide. The electrical measurements were performed with the support of the Balard Plateforme d’Analyses et de Caractérisation (PAC Balard). The authors acknowledge John Brown for his help in revising the manuscript.

References

1. X.-W. Liu, T.-J. Sun, J.-L. Hu and S.-D. Wang, *Journal of Materials Chemistry A*, 2016, **4**, 3584-3616.
2. Y. Zheng, S. Zheng, H. Xue and H. Pang, *Advanced Functional Materials*, 2018, **28**, 1804950.
3. M. Muschi and C. Serre, *Coordination Chemistry Reviews*, 2019, **387**, 262-272.
4. X. Zhou, W. Huang, J. Liu, H. Wang and Z. Li, *Chemical Engineering Science*, 2017, **167**, 98-104.
5. Y. Cao, Y. Zhao, Z. Lv, F. Song and Q. Zhong, *Journal of Industrial and Engineering Chemistry*, 2015, **27**, 102-107.
6. R. Kumar, D. Raut, U. Ramamurty and C. N. R. Rao, *Angewandte Chemie International Edition*, 2016, **55**, 7857-7861.
7. K. Jayaramulu, K. K. R. Datta, C. Rösler, M. Petr, M. Otyepka, R. Zboril and R. A. Fischer, *Angewandte Chemie International Edition*, 2016, **55**, 1178-1182.
8. C. A. Trickett, A. Helal, B. A. Al-Maythalony, Z. H. Yamani, K. E. Cordova and O. M. Yaghi, *Nature Reviews Materials*, 2017, **2**, 17045.
9. K. Adil, P. M. Bhatt, Y. Belmabkhout, S. M. T. Abtab, H. Jiang, A. H. Assen, A. Mallick, A. Cadiau, J. Aqil and M. Eddaoudi, *Advanced Materials*, 2017, **29**, 1702953.
10. C. A. Grande and A. E. Rodrigues, *International Journal of Greenhouse Gas Control*, 2008, **2**, 194-202.
11. T. Chronopoulos, Y. Fernandez-Diez, M. M. Maroto-Valer, R. Ocone and D. A. Reay, *Microporous and Mesoporous Materials*, 2014, **197**, 288-290.
12. E. J. Lee, J. Bae, K. M. Choi and N. C. Jeong, *ACS Applied Materials & Interfaces*, 2019, **11**, 35155-35161.
13. L. S. Xie, G. Skorupskii and M. Dincă, *Chemical Reviews*, 2020, **120**, 8536-8580.
14. L. Sun, M. G. Campbell and M. Dincă, *Angewandte Chemie International Edition*, 2016, **55**, 3566-3579.
15. B. Quan, X. Liang, G. Ji, Y. Cheng, W. Liu, J. Ma, Y. Zhang, D. Li and G. Xu, *Journal of Alloys and Compounds*, 2017, **728**, 1065-1075.
16. C. Petit and T. J. Bandosz, *Journal of colloid and interface science*, 2015, **447**, 139-151.
17. X. Qiu, X. Wang and Y. Li, *Chemical Communications*, 2015, **51**, 3874-3877.
18. R. Kumar, K. Jayaramulu, T. K. Maji and C. N. R. Rao, *Chemical Communications*, 2013, **49**, 4947-4949.
19. R. Liang, L. Shen, F. Jing, N. Qin and L. Wu, *ACS Applied Materials & Interfaces*, 2015, **7**, 9507-9515.
20. M. Muschi, A. Lalitha, S. Sene, D. Aureau, M. Fregnaux, I. Esteve, L. Rivier, N. Ramsahye, S. Devautour-Vinot, C. Sicard, N. Menguy, C. Serre, G. Maurin and N. Steunou, *Angewandte Chemie International Edition*, 2020, **59**, 10353-10358.
21. V. Benoit, R. S. Pillai, A. Orsi, P. Normand, H. Jobic, F. Nouar, P. Billemont, E. Bloch, S. Bourrelly, T. Devic, P. A. Wright, G. de Weireld, C. Serre, G. Maurin and P. L. Llewellyn, *Journal of Materials Chemistry A*, 2016, **4**, 1383-1389.
22. C. Serre, J. A. Groves, P. Lightfoot, A. M. Z. Slawin, P. A. Wright, N. Stock, T. Bein, M. Haouas, F. Taulelle and G. Férey, *Chemistry of Materials*, 2006, **18**, 1451-1457.

23. Y. Hu, J. Wei, Y. Liang, H. Zhang, X. Zhang, W. Shen and H. Wang, *Angewandte Chemie International Edition*, 2016, **55**, 2048-2052.
24. N. A. Travlou, K. Singh, E. Rodriguez-Castellon and T. J. Bandosz, *Journal of Materials Chemistry A*, 2015, **3**, 11417-11429.
25. C. Petit and T. J. Bandosz, *Advanced Functional Materials*, 2011, **21**, 2108-2117.
26. S. Liu, L. Sun, F. Xu, J. Zhang, C. Jiao, F. Li, Z. Li, S. Wang, Z. Wang, X. Jiang, H. Zhou, L. Yang and C. Schick, *Energy & Environmental Science*, 2013, **6**, 818-823.
27. Y. Shen, Z. Li, L. Wang, Y. Ye, Q. Liu, X. Ma, Q. Chen, Z. Zhang and S. Xiang, *Journal of Materials Chemistry A*, 2015, **3**, 593-599.
28. X. Zhou, W. Huang, J. Shi, Z. Zhao, Q. Xia, Y. Li, H. Wang and Z. Li, *Journal of Materials Chemistry A*, 2014, **2**, 4722-4730.
29. Y. Zhou, Z. Mao, W. Wang, Z. Yang and X. Liu, *ACS Applied Materials & Interfaces*, 2016, **8**, 28904-28916.
30. N. Liu, W. Huang, X. Zhang, L. Tang, L. Wang, Y. Wang and M. Wu, *Applied Catalysis B: Environmental*, 2018, **221**, 119-128.
31. L. Shen, L. Huang, S. Liang, R. Liang, N. Qin and L. Wu, *RSC Advances*, 2014, **4**, 2546-2549.
32. M. Jahan, Z. Liu and K. P. Loh, *Advanced Functional Materials*, 2013, **23**, 5363-5372.
33. L. Yang, B. Tang and P. Wu, *Journal of Materials Chemistry A*, 2015, **3**, 15838-15842.
34. J. Wei, Y. Hu, Y. Liang, B. Kong, J. Zhang, J. Song, Q. Bao, G. P. Simon, S. P. Jiang and H. Wang, *Advanced Functional Materials*, 2015, **25**, 5768-5777.
35. Z. Lin, Y. Yao, Z. Li, Y. Liu, Z. Li and C.-P. Wong, *The Journal of Physical Chemistry C*, 2010, **114**, 14819-14825.
36. C. Mattevi, G. Eda, S. Agnoli, S. Miller, K. A. Mkhoyan, O. Celik, D. Mastrogiovanni, G. Granozzi, E. Garfunkel and M. Chhowalla, *Advanced Functional Materials*, 2009, **19**, 2577-2583.
37. B. Szczęśniak, J. Choma and M. Jaroniec, *Journal of colloid and interface science*, 2018, **514**, 801-813.
38. B. Chen, Y. Zhu and Y. Xia, *RSC Advances*, 2015, **5**, 30464-30471.
39. W. Li, C. Y. Chuah, Y. Yang and T.-H. Bae, *Microporous and Mesoporous Materials*, 2018, **265**, 35-42.
40. S. Biswas, J. Zhang, Z. Li, Y.-Y. Liu, M. Grzywa, L. Sun, D. Volkmer and P. Van Der Voort, *Dalton Transactions*, 2013, **42**, 4730-4737.
41. F. Ragon, B. Campo, Q. Yang, C. Martineau, A. D. Wiersum, A. Lago, V. Guillerm, C. Hemsley, J. F. Eubank, M. Vishnuvarthan, F. Taulelle, P. Horcajada, A. Vimont, P. L. Llewellyn, M. Daturi, S. Devautour-Vinot, G. Maurin, C. Serre, T. Devic and G. Clet, *Journal of Materials Chemistry A*, 2015, **3**, 3294-3309.
42. S. Biswas and P. Van Der Voort, *European Journal of Inorganic Chemistry*, 2013, **2013**, 2154-2160.